



# One-dimensional soil moisture profile retrieval by assimilation of near-surface observations: a comparison of retrieval algorithms

Jeffrey P. Walker \*, Garry R. Willgoose, Jetse D. Kalma

*Department of Civil, Surveying and Environmental Engineering, The University of Newcastle, Callaghan, NSW 2308, Australia*

Received 28 March 2000; accepted 6 July 2000

## Abstract

This paper investigates the ability to retrieve the true soil moisture and temperature profiles by assimilating near-surface soil moisture and surface temperature data into a soil moisture and heat transfer model. The direct insertion and Kalman filter assimilation schemes have been used most frequently in assimilation studies, but no comparisons of these schemes have been made. This study investigates which of these approaches is able to retrieve the soil moisture and temperature profiles the fastest, over what depth soil moisture observations are required, and the effect of update interval on profile retrieval. These questions are addressed by a desktop study using synthetic data. The study shows that the Kalman filter assimilation scheme is superior to the direct insertion assimilation scheme, with retrieval of the soil moisture profile being achieved in 12 h as compared to 8 days or more, depending on observation depth, for hourly observations. It was also found that profile retrieval could not be realised for direct insertion of the surface node alone, and that observation depth does not have a significant effect on profile retrieval time for the Kalman filter. The observation interval was found to be unimportant for profile retrieval with the Kalman filter when the forcing data is accurate, whilst for direct insertion the continuous Dirichlet boundary condition was required for an increasingly longer period of time. It was also found that the Kalman filter assimilation scheme was less susceptible to unstable updates if volumetric soil moisture was modelled as the dependent state rather than matric head, because the volumetric soil moisture state is more linear in the forecasting model. © 2000 Elsevier Science Ltd. All rights reserved.

## 1. Introduction

The role of soil moisture in the shallow layers known as the root zone is widely recognised as a key parameter in numerous environmental studies, including: (i) meteorology; (ii) hydrology; and (iii) agriculture. The significance of soil moisture in these fields of study is its role in the partitioning of available energy at the ground surface into sensible and latent heat exchange with the atmosphere (thus controlling evapotranspiration) and in partitioning of precipitation into infiltration and runoff [13,18,24]. Furthermore, soil moisture is one of the few directly observable hydrological variables that plays an important part in the water and energy budgets necessary for climate studies [22]. Adequate knowledge of the soil moisture as well as the evapotranspiration rate at the land surface, which is dependent on the moisture

state below the shallow depth that controls the instantaneous response [12], is essential to the understanding and prediction of the reciprocal influences between land surface processes, weather and climate [40]. In agriculture, accurate assessment of soil moisture conditions is necessary for good water management, allowing rational planning of irrigation scheduling [21,25] and increased crop yields [23,38,41]. In addition, many insects and diseases are soil moisture dependent in hatching and spreading [10]. Therefore a detailed knowledge of soil moisture values over an area will allow pesticides to be applied selectively with obvious economic and environmental benefits [10]. It has also been noted that the denitrification rate of soil is related to soil moisture [1], and that areas of high sediment transport are related to runoff producing zones [3].

Soil moisture can be estimated from: (i) point measurements; (ii) hydrologic models; and (iii) remote sensing. The traditional point measurement techniques for soil moisture estimation do not always represent the spatial distribution [25] as there is a limited area that can be satisfactorily monitored with an acceptable temporal

\* Corresponding author. Present address: NASA-GSFC/Universities Space Research Association, Rm B309, Building 3, Mail Code 974, Greenbelt, MD 20771, USA.

E-mail address: cejpw@land.gsfc.nasa.gov (J.P. Walker).

resolution. Moreover, soil moisture is highly variable with a very low spatial correlation [9,18]. The alternative has been to estimate the spatial distribution of soil moisture using a distributed hydrologic model [14,30]. However, estimates with such models are generally poor, because soil moisture exhibits large spatial and temporal variation [11] as a result of inhomogeneity of soil properties, vegetation and precipitation [29]. As remote sensing can be used to collect spatial data over large areas on a routine basis, it provides a capability to make frequent and spatially comprehensive measurements of the near-surface soil moisture [11,23]. However, major limitations with current satellite data are: (i) the number of days between overpasses of the same point on the ground; and (ii) the depth of the soil moisture measurement, being limited typically to the top few centimetres [11,24,39]. These upper few centimetres of the soil are the most exposed to the atmosphere, and their soil moisture varies rapidly in response to rainfall and evaporation [22]. Thus to be useful for hydrologic, climatic and agricultural studies, these observations of near-surface soil moisture must be related to the complete soil moisture profile in the unsaturated zone [20,31,34].

Given the inherent problems and complimentary nature of point measurements, hydrological modelling and remote sensing in determining the spatial distribution and temporal variation of soil moisture profiles, an effective soil moisture monitoring program should combine these three approaches. Point measurements, which are the most accurate, would be used sparingly for calibration and evaluation of the hydrologic model, which yields information on both the spatial (horizontal and vertical) distribution and temporal variation of soil moisture content. Remote sensing observations, which provide a measurement of the near-surface soil moisture content, would be used for updating of the hydrologic model by data assimilation, to minimise the effects of errors in the model physics and input data (model parameters and atmospheric forcing).

Only a small number of studies have attempted to use remotely sensed near-surface soil moisture measurements as either input to a hydrologic model, or as verification data [4]. The reasons for this are: (i) remote sensing data is just beginning to gain acceptance in the hydrologic community as an operational tool for measuring the near-surface soil moisture; and (ii) assimilation of remote sensing data requires the development of hydrological models that simulate soil moisture for a thin near-surface layer that is compatible with the nature of the remote sensing observations [28]. In addition, techniques for assimilating the remote sensing data into the hydrologic model require investigation, and the near-surface soil moisture observations must be proven useful when used with hydrologic models [16].

With the exception of only a few studies, previous studies have assimilated near-surface soil moisture observations into a hydrologic model with the objective to improve predictions of evapotranspiration or runoff, or have estimated the soil moisture profile for a one-dimensional soil column using synthetic data and a very short (i.e. 1 h) update interval [13]. Furthermore, with one exception [19], there has been no assessment of the various assimilation schemes available for updating the hydrologic model. Moreover, there has been no study on the effect of observation depth and update interval. This paper explores the effects of observation depth and update interval on soil moisture profile retrieval and makes a comparison of two commonly used assimilation techniques (direct insertion and Kalman filter) in a desktop study using synthetic data, and provides a result in that respect. As this is a synthetic study, the implicit assumption is a perfect model with perfect parameters, perfect forcing and perfect observations, the only uncertainty being the initial condition. However, in a “real world” application there is uncertainty associated with all aspects of the assimilation system.

In the recent studies of Entekhabi et al. [12,13], a brightness temperature model and coupled soil moisture and heat transfer model have been combined in the context of a Kalman filter for a one-dimensional soil column. The Kalman filter is a statistical assimilation scheme that updates the model state values based on the relative magnitudes of the covariances of both the model state and the observation. The model update was made using infra-red and low frequency vertical and horizontal polarisation passive microwave observations. The algorithm was tested using synthetic data from a drying period, with “true” soil moisture and temperature profiles generated from the same coupled heat and moisture transfer model as used in the Kalman filter. Remote sensing observations were then generated from these profiles, and used to update the system state equations each hour. Starting from a poor initial guess of the soil moisture profile, the Kalman filter estimate of the soil moisture profile was found to correspond with the true profile after approximately 5 days. This approach was recently tested for an 8-day field experiment with daily updation and a 4-month synthetic study with updation every 3 days [15].

The feasibility of updating the three-layer TOPLATS model using several alternative assimilation schemes has been investigated by Houser et al. [19] in a field study. The schemes investigated were: (i) direct insertion; (ii) statistical correction; (iii) Newtonian nudging; and (iv) statistical interpolation. Direct insertion replaces the model state values with the observed values directly, while the other schemes use a statistical technique to make the update. In the statistical correction scheme the modelled state mean and standard deviation are adjusted to match the observed mean and standard devi-

ation, while Newtonian nudging (a special and typically pathological case of the Kalman filter) relaxes the model state towards the observed state by adding a term to the prognostic equation that is proportional to the difference between the two states, and statistical interpolation is a minimum variance method that is closely related to kriging. It was found that none of these schemes produced time series that matched the root zone observations. However, Newtonian nudging made the largest impact on root zone soil moisture while statistical interpolation had a relatively strong influence on root zone soil moisture.

## 2. Microwave remote sensing

The fundamental basis of microwave remote sensing for soil moisture is the relationship between soil dielectric properties and volumetric soil moisture content [24]. In addition to its strong dependence on volumetric soil moisture, the magnitude of the dielectric constant is a function of the observation frequency, soil temperature, soil texture and soil bulk density. However, the dependence on soil temperature is often ignored. To highlight the importance of soil temperature on the dielectric constant, the dielectric mixing model of Peplinski et al. [35] has been evaluated for two soil moisture conditions and several soil temperatures over a range of observation frequencies, with the results given in Fig. 1.

Soil temperature in the near surface layer can have a diurnal variation of more than 30–40°C in some parts of the world. Fig. 1 indicates that temperature variations of this magnitude have a significant effect on the magnitude of both the real and imaginary components of the soil dielectric constant, especially at high soil moisture. This emphasises the need for an estimate of soil temperature in the surface layer if remote sensing observations are to be used for measuring near-surface soil moisture. As current generation microwave remote sensing platforms do not carry a thermal infra-red sensor, estimation of

surface soil temperature is required from alternate means. In this paper, it is suggested that soil temperature be estimated from the temperature component of a coupled soil moisture and heat transfer model, which is updated with thermal infra-red observations from another remote sensing platform.

## 3. Retrieval algorithms

### 3.1. Direct insertion

The direct insertion assimilation is performed by directly substituting observed values for the simulated values of soil moisture and temperature as they become available (Fig. 2(a)). Infra-red remote sensing observations only provide information on the soil skin temperature, so only the soil temperature of the surface node in the soil discretisation may be updated. In contrast, microwave remote sensing observations of soil moisture are related to the soil moisture in a layer as thick as a few tenths of the wavelength [11,24,39]. The thickness of this layer is referred to as the observation depth [43].

The governing equations for flow of heat and moisture through unsaturated soil, and the theoretical equations relating microwave observations to soil moisture, are highly nonlinear. Therefore the direct insertion assimilation scheme is simpler than the Kalman filter algorithm below, as it allows the nonlinear problem to be solved directly. However, the only way in which this surface information is transferred to deeper layers is through the infiltration and exfiltration processes described by the physics of the soil moisture model. Moreover, the soil moisture profile is only changed by the difference between the observed and simulated soil moisture, limiting the ability of the direct insertion to correct an erroneous mass balance.

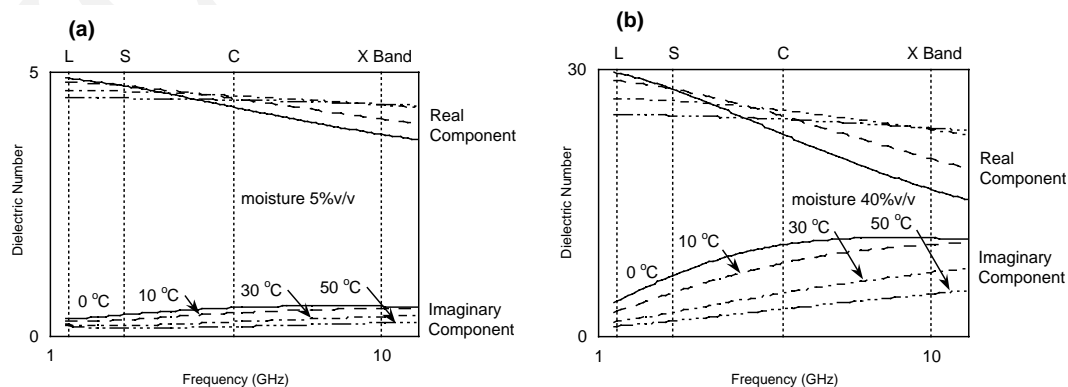


Fig. 1. Temperature dependence of dielectric constant number: (a) low soil moisture and (b) high soil moisture.

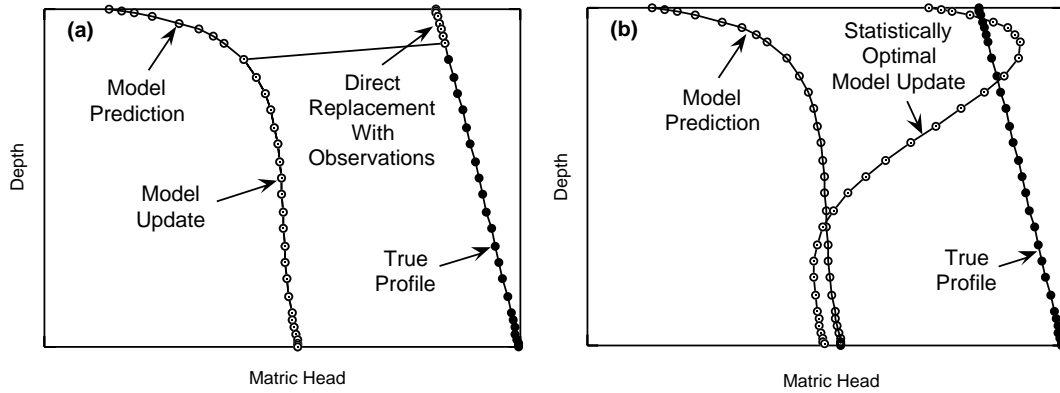


Fig. 2. Illustration of data assimilation techniques: (a) direct insertion and (b) Kalman filter.

### 3.2. The (extended) Kalman filter

The Kalman filter is a statistical assimilation technique that updates the profile based on the relative magnitudes of the covariances of both the observations and the model profile estimate. The principal advantage of the Kalman filter is that the entire profile may be modified (Fig. 2(b)) because of the correlation between the soil moisture near the surface and at deeper depths. The disadvantages of this approach are that the governing equations require linearisation and that it is computationally intensive when large systems are involved.

The Kalman filter algorithm tracks the conditional mean of a statistically optimal estimate of a state vector  $\mathbf{X}$ , through a series of propagation and update steps [5]. For this application, the state vector defines the system state of the soil as  $\mathbf{X} = \{\psi_1, \psi_2, \dots, \psi_N : T_1, T_2, \dots, T_N\}^T$ , where  $\psi_j$  is the soil matric head at node  $j$  and  $T_j$  is the soil temperature at node  $j$ . To apply the Kalman filter approach, the nonlinear equations governing soil moisture and heat transfer must be written as in the linear state space equation form of Eq. (1), termed the extended Kalman filter. During the forecasting period, the covariances of the system states are also estimated, using Eq. (2). The forecasting equations are:

$$\hat{\mathbf{X}}^{n+1/n} = \mathbf{A}^n \cdot \hat{\mathbf{X}}^{n/n} + \mathbf{U}^n + \mathbf{w}^n, \quad (1)$$

$$\Sigma_x^{n+1/n} = \mathbf{A}^n \cdot \Sigma_x^{n/n} \cdot \mathbf{A}^{nT} + \mathbf{Q}, \quad (2)$$

where  $\mathbf{A}$  is a matrix relating the system states at time  $n + 1$  to the system state at time  $n$ ,  $\mathbf{U}$  a vector of forcing,  $\mathbf{w}$  the model error,  $\Sigma_x$  the covariance matrix of the system states and  $\mathbf{Q}$  is the covariance matrix of the system noise (i.e.  $E[\mathbf{w} \cdot \mathbf{w}^T]$ ).

Given the initial state vector  $\hat{\mathbf{X}}^{0/0}$  and its covariance matrix  $\Sigma_x^{0/0}$ , the soil states may be forecast (denoted by the time superscript  $(n + 1)/n$ ) using Eqs. (1) and (2) until a set of observations become available, at which

stage a system update may be made (denoted by the time superscript  $(n + 1)/(n + 1)$ ).

For the update step, the observation equation is written such that observation vector  $\mathbf{Z}$  is a linear function of the state vector  $\mathbf{X}$

$$\mathbf{Z} = \mathbf{H} \cdot \mathbf{X} + \mathbf{v}, \quad (3a)$$

where  $\mathbf{v}$  is the observation error with covariance matrix  $\mathbf{R}$ . Since microwave remote sensing observations are nonlinearly related to the soil moisture content, the simplest way to make the update is to invert the observations for soil moisture down to the observation depth  $d$ . This reduces the need for linearisation of the dielectric and backscattering/brightness temperature models, eliminating errors introduced through linearisation. Subsequently the observation equation becomes

$$\begin{Bmatrix} \psi_1 \\ \psi_2 \\ \vdots \\ \psi_d \\ \vdots \\ \psi_{N-1} \\ \psi_N \\ T_1 \\ T_2 \\ \vdots \\ T_{N-1} \\ T_N \end{Bmatrix} = \begin{bmatrix} 1 & 0 & \dots & 0 & \dots & 0 & 0 & \dots & 0 & 0 & \dots & 0 & 0 \\ 0 & 1 & \dots & 0 & \dots & 0 & 0 & \dots & 0 & 0 & \dots & 0 & 0 \\ \vdots & \vdots & \ddots & \vdots & \ddots & \vdots & \vdots & \vdots & \ddots & \vdots & \vdots & \vdots & \vdots \\ 0 & 0 & \dots & 1 & \dots & 0 & 0 & \dots & 0 & 0 & \dots & 0 & 0 \\ \dots & \dots \\ 0 & 0 & \dots & 0 & \dots & 0 & 0 & \dots & 1 & 0 & \dots & 0 & 0 \end{bmatrix} + \mathbf{v} \quad (3b)$$

where  $T_1$  is the surface soil temperature estimated from infra-red observations and  $\psi_d$  is the soil matric suction at the observation depth  $d$ . This form of the observation equation allows the updating to be performed using either direct measurements of near-surface soil moisture or by inverting any algorithm that relates soil moisture

to remote sensing observations. This is a key difference between the present study and the Kalman filter studies of Entekhabi et al. [13] and Galantowicz et al. [15].

Updating of the system state vector  $\hat{\mathbf{X}}$  with the observations  $\mathbf{Z}$  is performed by

$$\hat{\mathbf{X}}^{n+1/n+1} = \hat{\mathbf{X}}^{n+1/n} + \mathbf{K}^{n+1} \left( \mathbf{Z}^{n+1} - \mathbf{H}^{n+1} \cdot \hat{\mathbf{X}}^{n+1/n} \right), \quad (4)$$

$$\Sigma_x^{n+1/n+1} = (\mathbf{I} - \mathbf{K}^{n+1} \cdot \mathbf{H}^{n+1}) \cdot \Sigma_x^{n+1/n}, \quad (5)$$

where  $\mathbf{I}$  is the identity matrix. The Kalman gain matrix  $\mathbf{K}^{n+1}$  weights the observation against the model forecast by the relative magnitudes of model covariances ( $\Sigma_x^{n+1/n}$ ) and the observation covariances ( $\mathbf{R}^{n+1}$ ). The Kalman gain is

$$\mathbf{K}^{n+1} = \Sigma_x^{n+1/n} \cdot \mathbf{H}^{n+1\text{T}} \cdot \left( \mathbf{R}^{n+1} + \mathbf{H}^{n+1} \cdot \Sigma_x^{n+1/n} \cdot \mathbf{H}^{n+1\text{T}} \right)^{-1}. \quad (6)$$

The derivation of these expressions are given by Bras and Rodriguez-Iturbe [5].

The key assumptions of the Kalman filter are that: (i) the model error  $\mathbf{w}$  is Gaussian white noise with a mean vector equal to zero and covariance matrix equal to  $\mathbf{Q}$ ; (ii) the observation error  $\mathbf{v}$  is Gaussian white noise with mean equal to zero and variance equal to  $\mathbf{R}$ ; and (iii) the initial state vector  $\hat{\mathbf{X}}^{0/0}$  is Gaussian with mean  $\hat{\mathbf{X}}^{0/0}$  and covariance  $\Sigma_x^{0/0}$ .

Model errors result from: (i) inaccurate specification of the model structure; (ii) linearisation of the model physics; (iii) estimation errors in the values of model parameters; and (iv) measurement errors in model inputs (precipitation and evapotranspiration). Degree-of-belief estimates of the errors in initial states and parameters can be used to specify the diagonal elements of these covariance parameter vectors with the off-diagonal elements set to zero. The observation variance  $\mathbf{R}$  can be identified reliably in most cases, since it depends on the characteristics of the measuring device [17].

#### 4. Soil moisture and heat transfer equations

The coupled flow of heat and moisture in a vertical soil column occurs in both vapour and liquid phases. The relative magnitudes of vapour versus liquid fluxes and the effects of temperature versus hydraulic gradients are not well understood [27]. While some authors (e.g. Cary and Taylor [6]) consider temperature effects very important over a wide range of soil wetness, others (e.g. Philip [36]) indicate that thermally driven flow in the evaporative drying may be of minor importance until the soil becomes very dry. Kimball et al. [26] conclude, based on a comparison study of field measured and calculated soil heat fluxes, that both soil water and heat flux can be better predicted by ignoring thermal vapour movement at high and low water contents. At interme-

diated water contents, soil water flux prediction is better if thermal vapour flux is included. The vapour phase is mainly critical in modelling the thermal regime due to the relatively large magnitude of heat exchange during phase change. For moisture flow, however, the vapour term is orders of magnitude smaller than the liquid flux and may thus be neglected [13]. As the soil temperature profile is only of secondary importance here, we consider the liquid phase only. The coupling between the heat and moisture equations will be solely through the heat capacity of the soil and through the influence of moisture on thermal conductivity.

##### 4.1. Moisture equation

The conservation of water mass in a porous medium can be expressed by the continuity equation for one-dimensional simultaneous saturated-unsaturated flow as

$$\frac{\partial S_\theta}{\partial t} = -\nabla q_m, \quad (7)$$

where  $q_m$  is the total mass flux of water given by  $q_m = q_l + q_v$  where  $q_l$  is the mass flux of liquid water and  $q_v$  is the mass flux of water vapour and  $S_\theta$  is the mass of water storage per unit bulk volume [2]

$$S_\theta = \rho_l(\theta_l + \theta_v) = \rho_l\theta \quad (8a)$$

or

$$S_\theta = \rho_l\phi S_w, \quad (8b)$$

where  $\rho_l$  is the density of liquid water,  $\theta_l$  the volumetric liquid water content,  $\theta_v$  the volumetric water vapour content,  $\phi$  is the soil porosity and  $S_w$  is the water saturation equal to  $\theta/\phi$ .

Differentiating Eq. (8b) with respect to time yields [2]

$$\frac{\partial S_\theta}{\partial t} = \rho_l \left\{ S_w S_{0\psi} \frac{\partial \psi}{\partial t} + \frac{\partial \theta}{\partial t} \right\}, \quad (9)$$

where  $\psi$  is the soil water matric potential, otherwise known as the capillary potential.  $S_{0\psi}$  is the specific storativity with respect to soil matric potential given by

$$S_{0\psi} = \alpha(1 - \phi) + \beta\phi. \quad (10)$$

Following Philip and de Vries [37] and de Vries [7], the respective equations for liquid and vapour flux densities are:

$$\frac{q_l}{\rho_l} = -D_{\psi l} \nabla(\psi + z) - D_{Tl} \nabla T, \quad (11a)$$

$$\frac{q_v}{\rho_l} = -D_{\psi v} \nabla \psi - D_{Tv} \nabla T, \quad (11b)$$

for elevation  $z$  positive upward. The dependent variables are the soil water matric potential  $\psi$  and the soil temperature  $T$ . The transport coefficients are the isothermal liquid hydraulic conductivity  $D_{\psi l}$ , the thermal liquid diffusivity  $D_{Tl}$ , the isothermal vapour conductivity  $D_{\psi v}$  and the thermal vapour diffusivity  $D_{Tv}$ . Substitution of

Eqs. (9), (11a) and (11b) into Eq. (7) and assuming that  $\nabla_{\rho_1}$  is zero yields the mixed form of the governing equation for flow of soil moisture in both the liquid and vapour phases under both moisture and temperature gradients

$$S_w S_{0\psi} \frac{\partial \psi}{\partial t} + \frac{\partial \theta}{\partial t} = \nabla [D_\psi \nabla \psi + D_T \nabla T + D_{\psi 1}], \quad (12)$$

where the transport coefficients are the isothermal moisture conductivity  $D_\psi = D_{\psi 1} + D_{\psi v}$  and the thermal moisture diffusivity  $D_T = D_{T1} + D_{Tv}$ .

In order to satisfy the required form of the linear state space equation, the moisture equation must be in either the  $\theta$ -based or  $\psi$ -based form, which may be obtained by inclusion of the soil capillary capacity factor  $C_\psi = \partial \theta / \partial \psi$ . One important advantage of the  $\theta$ -based form of the governing equation is that the mass balance of the system is guaranteed during the moisture forecasting period, regardless of discretisation and time step size, with only its distribution throughout the profile being affected [33]. However, the  $\theta$ -based form cannot be used to model multi-layered soils. The reason for this is that the soil's hydraulic potential must be continuous across the interface between each layer, while the moisture content can vary. Furthermore, the  $\psi$ -based form facilitates modelling of soil systems that are locally saturated [33]. Thus, it is desirable to write the soil moisture equation in the  $\psi$ -based form.

By neglecting the vapour flux and considering a purely isothermal situation, the following relationship for one-dimensional saturated–unsaturated flow through porous media is obtained

$$(S_w S_{0\psi} + C_\psi) \frac{\partial \psi}{\partial t} = \nabla [D_{\psi 1} \nabla \psi + D_{\psi 1}], \quad (13)$$

where the isothermal liquid hydraulic conductivity  $D_{\psi 1}$  is simply the unsaturated hydraulic conductivity. Writing Eq. (13) in explicit finite difference form for node  $j$  at time step  $n + 1$  and vectorising yields:

$$\{\psi_j\}^{n+1} = \left\{ \begin{array}{l} \frac{(t^{n+1} - t^n) (D_{\psi 1_{j-1}}^n + D_{\psi 1_j}^n)}{(S_{w_j}^n S_{0\psi_j}^n + C_{\psi_j}^n) (z_{j-1} - z_{j+1}) (z_{j-1} - z_j)} \\ 1 - \frac{(t^{n+1} - t^n)}{(S_{w_j}^n S_{0\psi_j}^n + C_{\psi_j}^n) (z_{j-1} - z_{j+1})} \left[ \frac{D_{\psi 1_{j-1}}^n + D_{\psi 1_j}^n}{z_{j-1} - z_j} + \frac{D_{\psi 1_j}^n + D_{\psi 1_{j+1}}^n}{z_j - z_{j+1}} \right] \\ \frac{(t^{n+1} - t^n) (D_{\psi 1_j}^n + D_{\psi 1_{j+1}}^n)}{(S_{w_j}^n S_{0\psi_j}^n + C_{\psi_j}^n) (z_{j-1} - z_{j+1}) (z_j - z_{j+1})} \end{array} \right\}^T \times \left\{ \begin{array}{l} \psi_{j-1} \\ \psi_j \\ \psi_{j+1} \end{array} \right\}^n + \left\{ \left( \frac{t^{n+1} - t^n}{S_{w_j}^n S_{0\psi_j}^n + C_{\psi_j}^n} \right) \left( \frac{D_{\psi 1_{j-1}}^n - D_{\psi 1_{j+1}}^n}{z_{j-1} - z_{j+1}} \right) \right\}. \quad (14)$$

## 4.2. Temperature equation

The conservation of heat content in a porous medium can be expressed by the continuity equation for one-dimensional heat transfer as

$$\frac{\partial S_h}{\partial t} = -\nabla q_h, \quad (15)$$

where  $q_h$  is the heat flux density.  $S_h$  is the total heat content per unit bulk volume and has been expressed by de Vries [7] as

$$S_h = (C_d + c_1 \rho_1 \theta_1 + c_p \rho_1 \theta_v) (T - T_{\text{ref}}) + L_{\text{ref}} \rho_1 \theta_v - \rho_1 \int_0^{\theta_1} W d\theta_1, \quad (16)$$

where  $C_d$  is the volumetric heat capacity of the dry soil,  $c_1$  and  $c_p$  the specific heat capacity of liquid water and water vapour, respectively (at constant pressure),  $T_{\text{ref}}$  an arbitrary reference temperature,  $L_{\text{ref}}$  the latent heat of vaporisation at temperature  $T_{\text{ref}}$ , and  $W$  is the differential heat of wetting.

Ignoring the contribution to heat storage from the differential heat of wetting, the rate of change of heat storage with time can be written as:

$$\begin{aligned} \frac{\partial S_h}{\partial t} &= (C_d + c_1 \rho_1 \theta_1 + c_p \rho_1 \theta_v) \frac{\partial T}{\partial t} \\ &+ \left( c_1 \rho_1 \frac{\partial \theta_1}{\partial t} + c_p \rho_1 \frac{\partial \theta_v}{\partial t} \right) (T - T_{\text{ref}}) \\ &+ L_{\text{ref}} \rho_1 \frac{\partial \theta_v}{\partial t}. \end{aligned} \quad (17)$$

Following de Vries [7], the total heat flux density for both sensible and latent heat in a porous medium is

$$q_h = -(\lambda - L \rho_1 D_{Tv}) \nabla T + L q_v + c_1 (T - T_{\text{ref}}) q_m, \quad (18)$$

where  $L$  is the latent heat of vaporisation of water at temperature  $T$  and  $\lambda$  is the thermal conductivity.

Therefore, substitution of Eqs. (17) and (18) into Eq. (15) yields the governing equation for heat transfer in a one-dimensional soil column

$$\begin{aligned} C_T \frac{\partial T}{\partial t} &= \nabla [(\lambda - \rho_1 D_{Tv} L) \nabla T - L q_v - c_1 (T - T_{\text{ref}}) q_m] \\ &- \left( c_1 \rho_1 \frac{\partial \theta_1}{\partial t} + c_p \rho_1 \frac{\partial \theta_v}{\partial t} \right) (T - T_{\text{ref}}) \\ &- L_{\text{ref}} \rho_1 \frac{\partial \theta_v}{\partial t}, \end{aligned} \quad (19)$$

where  $C_T = C_d + c_1 \rho_1 \theta_1 + c_p \rho_1 \theta_v$  is the volumetric heat capacity of the bulk soil medium [8]. By neglecting the vapour flux, the governing equation for heat transport in a porous medium may be reduced to

$$C_T \frac{\partial T}{\partial t} = \nabla [\lambda \nabla T - c_1 (T - T_{\text{ref}}) q_1] - c_1 \rho_1 (T - T_{\text{ref}}) \frac{\partial \theta_1}{\partial t}. \quad (20)$$

Writing Eq. (20) in explicit finite difference form for node  $j$  at time step  $n + 1$  and vectorising yields:

$$\{T_j\}^{n+1} = \left\{ \begin{array}{l} \frac{(t^{n+1}-t^n)(\lambda_{j-1}^n+\lambda_j^n)}{C_{T_j}^n(z_{j-1}-z_{j+1})(z_{j-1}-z_j)} - \frac{(t^{n+1}-t^n)c_1q_{1j-1}^n}{C_{T_j}^n(z_{j-1}-z_{j+1})} \\ 1 - \left( \frac{(t^{n+1}-t^n)}{C_{T_j}^n(z_{j-1}-z_{j+1})} \left[ \frac{\lambda_{j-1}^n+\lambda_j^n}{z_{j-1}-z_j} + \frac{\lambda_j^n+\lambda_{j+1}^n}{z_j-z_{j+1}} \right] \right) \\ - \frac{(t^{n+1}-t^n)c_1\rho_1}{C_{T_j}^n} \left[ \frac{\theta_{1j}^n-\theta_{1j}^{n-1}}{t^n-t^{n-1}} \right] \\ \frac{(t^{n+1}-t^n)(\lambda_j^n+\lambda_{j+1}^n)}{C_{T_j}^n(z_{j-1}-z_{j+1})(z_j-z_{j+1})} + \frac{(t^{n+1}-t^n)c_1q_{1j+1}^n}{C_{T_j}^n(z_{j-1}-z_{j+1})} \\ + \left\{ \frac{(t^{n+1}-t^n)c_1T_{\text{ref}}}{C_{T_j}^n} \left[ \frac{q_{1j-1}^n-q_{1j+1}^n}{z_{j-1}-z_{j+1}} \right] \right. \\ \left. + \frac{(t^{n+1}-t^n)c_1\rho_1T_{\text{ref}}}{C_{T_j}^n} \left[ \frac{\theta_{1j}^n-\theta_{1j}^{n-1}}{t^n-t^{n-1}} \right] \right\} \end{array} \right\}^T \left\{ \begin{array}{l} T_{j-1} \\ T_j \\ T_{j+1} \end{array} \right\}^n \quad (21)$$

## 5. Synthetic study

In order to explore the relative merits of the two data assimilation schemes and the effect of observation depth and frequency, a desktop study is presented using synthetic data. Synthetic data sets were generated using the same soil moisture and heat transfer model used to retrieve the profile data from surface observations. This eliminated experimental errors in measuring the soil moisture and temperature profiles, as well as in estimating the soil properties and surface fluxes. Furthermore, using the same model for generation and retrieval of profile data eliminated model errors due to the neglect of hysteresis, thermally induced moisture transport, heat of wetting and vapour components of the soil heat and moisture balance.

From a theoretical view point, more comprehensive models accounting for simultaneous heat and water transport could be used, but it would not markedly change the demonstration, as we use the same model to produce the simulated data and to process these data. However, the complexity of such models, the difficulty to obtain proper soil parameters for vapour flux, and the lack of knowledge about their spatial variability would probably make illusory the increase in accuracy expected by using such comprehensive models in the application we are dealing with. In the same way, hysteresis of the unsaturated hydraulic conductivity relationship has been neglected because of its small influence on the water transfer compared to the effect of the field variability of soil water characteristics.

### 5.1. Synthetic data

The soil moisture and heat transfer model described above was used to generate 40 days of true soil moisture and temperature profiles using the van Genuchten [42] moisture retention and hydraulic conductivity relation-

ships. The true soil moisture and temperature profiles were generated using the soil properties, initial conditions, and boundary conditions of Entekhabi et al. [13] to facilitate comparison with their retrieval algorithm. The soil parameters used by the model are given in Table 1. Initial conditions were  $-50$  cm matric head and  $20^\circ\text{C}$ , uniform throughout the 1 m deep soil profile. The time series of true profiles were generated by forcing the model with  $0.5$  cm day $^{-1}$  evaporation and a sinusoidal diurnal soil heat flux of  $200$  W m $^{-2}$  amplitude at the soil surface. The boundary condition at the base of the soil column was zero soil moisture and heat flux. To test the two assimilation schemes, the model was initialised with the same poor initial guess as used by Entekhabi et al. [13], that is, a uniform matric head of  $-300$  cm and soil temperature of  $15^\circ\text{C}$  throughout the profile.

### 5.2. Numerical experiments

In this study, both the direct insertion and Kalman filter assimilation schemes have been applied with a range of observation depths and update intervals, ranging from a continuously prescribed near-surface boundary condition (continuous Dirichlet boundary condition) to updating once every 5 days. When model updates are made at the soil surface using the direct insertion and Kalman filter approaches, the surface node(s) of the model are replaced with the observations, and the information contained in these observations is transferred to deeper depths through the physics of the model. Thus, these updating approaches are in some degree similar to the continuous Dirichlet boundary condition, at least for the period during which the updated surface node(s) remain close to the observation. For the soil moisture equation, the observation depths were taken to be 0 (surface node), 1, 4 and 10 cm, while for the temperature equation, the observation depth was taken as the surface node. The “observations” are the values from the true profiles for that time and depth. A summary of the simulations undertaken and the time for retrieval of the true profile for these simulations is given

Table 1  
Soil parameters used in validation

Total soil depth	100 cm
Number of nodes	31
Soil thermal and hydraulic parameters	Clay loam
	$K_s = 25$ cm/day
	$\phi = 0.54$
	$\theta_r = 0.2$
	$\eta = 0.008$
	$n = 1.8$
	Proportion quartz = 0.03
	Proportion other minerals = 0.41
	Proportion organic matter = 0.02
Initial conditions	$20^\circ\text{C}$ , $-50$ cm matric head

in Table 2. While simulations were undertaken for daily observations, these results are not discussed, as they are qualitatively similar to the results below.

### 5.3. Updating once every hour

In the initial testing, and to allow for comparison with the simulations of Entekhabi et al. [13], both the direct insertion and Kalman filter assimilation schemes were applied once every hour. The results from these simulations are given in Figs. 3 and 4 for direct insertion, and Figs. 5 and 6 for the Kalman filter. The true profiles are compared with the retrieved profiles as well as the open loop. Open loop is where no observations are used and the system is simply propagated from the initial conditions using the known surface fluxes.

For direct insertion, retrieved soil temperature profiles were found to differ only slightly for the various soil moisture observation depths (a result of heat capacity and thermal conductivity moisture dependence), while there were significant differences in the retrieved temperature profiles using the Kalman filter. Hence, the results for temperature profile retrieval using direct insertion are given for only the 4-cm soil moisture observation depth, for sake of clarity, while retrieved temperature profiles using the Kalman filter are given for all corresponding soil moisture observation depths. In addition, the retrieved profiles presented for direct insertion are for the timestep immediately prior to the update, whilst the retrieved profiles for the Kalman filter are immediately after the Kalman filter update. This is the situation for all direct insertion and Kalman filter simulations presented.

#### 5.3.1. Direct insertion

The direct insertion assimilation scheme performs an instantaneous replacement of the model estimate with the true soil moisture and temperature values over the observation depth every hour. Thus, the only way in which extra mass can be added to or removed from the system is through the observations at the surface nodes. It can be seen from both Fig. 3 for moisture retrieval using observations of the surface node and Fig. 4 for temperature retrieval, that if this information is provided for the surface node alone, then there is no profile retrieval and the system continues in the same fashion as the open loop. The reason for this is most likely that the model is driven by gradients, and the gradients at nodes below the surface node over-ride the update, rapidly replacing the update value with its original value. However, if the timestep size of the very first timestep after the update was increased by three orders of magnitude (10 s), then some of the updating information at the surface node was passed to deeper depths. The slight variation in the temperature profile from the open loop profile is a result of retrieval in soil moisture profiles, as soil heat capacity and soil thermal conductivity are a function of soil moisture. In addition, the soil temperature equation is a function of soil moisture and moisture flux.

The results from direct insertion of observations for depths greater than just the surface node indicate that profile retrieval proceeds more quickly as the observation depth is increased. This was also observed for a continuous Dirichlet boundary condition. However, the effect is much more pronounced in this instance. The reason for this may be that the continuous Dirichlet

Table 2  
Summary of profile retrieval simulations

	Direct insertion (days)				Soil temperature	Kalman filter (days)				Soil temperature
	Soil moisture					Soil moisture				
Observation depth (cm)	0	1	4	10	Surface	0	1	4	10	Surface
Update interval	Profile retrieval time (days)									
Continuous	8	8	7	5	> 20					
1 h	> 20	12	8	–	–	0.5	0.5	0.5	0.5	2
1 h <sup>a</sup>	–	> 20	16	10	–	0.7	0.7	0.7	0.7	2
1 day <sup>b</sup>		> 20	> 20	> 20	> 20					
1 day						3	3	3	3	6
5 days <sup>c</sup>		> 40	> 40	40	40					
5 days <sup>d</sup>						10	10	10	10	15
5 days <sup>e</sup>						–	10	–	–	
5 days <sup>f</sup>						–	15	15	10	

<sup>a</sup> Gravity drainage and advection boundary condition at base of soil column.

<sup>b</sup> Dirichlet boundary condition at soil surface for 1 h after update.

<sup>c</sup> Dirichlet boundary condition at soil surface for 1 day after update.

<sup>d</sup> Quasi observations applied to remainder of profile.

<sup>e</sup> Log transformation.

<sup>f</sup> Moisture transformation.

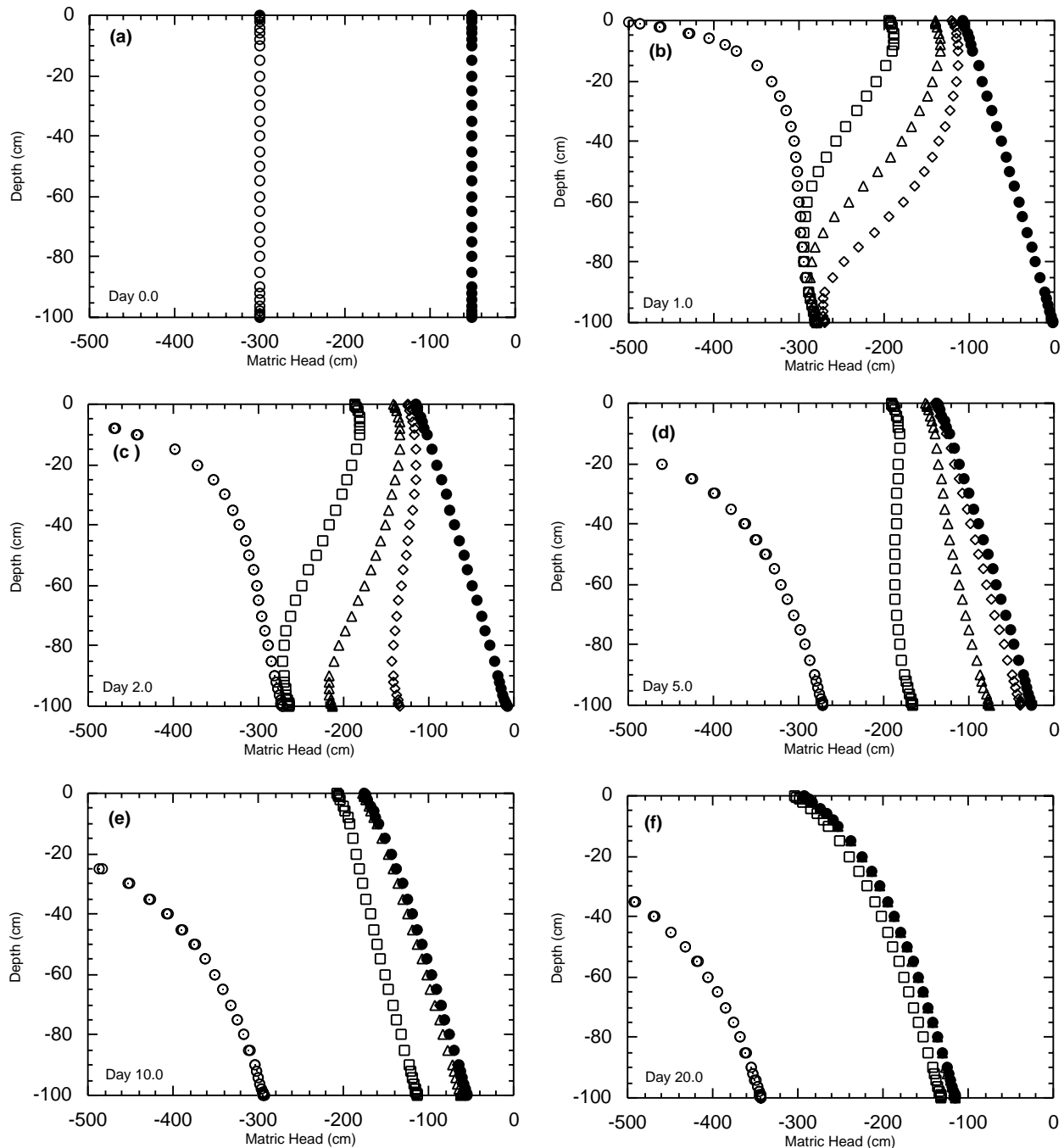


Fig. 3. Comparison of simulated soil moisture profiles using direct insertion for observation depths of 0 (open circle), 1 (open square), 4 (open triangle) and 10 cm (open diamond) with the true soil moisture profile (solid circle) and the open loop soil moisture profile (open circle with dot) for hourly observations. Soil moisture with depth for times after the beginning of simulation: (a) time zero, (b) 1 day, (c) 2 days, (d) 5 days, (e) 10 days and (f) 20 days.

boundary condition essentially controls the rate of moisture flux near the surface, with the depth over which the continuous Dirichlet boundary condition is applied controlling the depth at which this flux is applied. Thus for deeper depths, the flux is applied deeper within the soil column, resulting in a slightly reduced distance for propagation of this boundary condition

into the profile and hence a slightly faster adjustment. The direct insertion on the other hand is an instantaneous adjustment of the surface nodes, only controlling the rate of flux near the surface initially. This update information is redistributed to deeper depths relatively quickly, with the surface moisture and fluxes returning closely to their original values. More importantly how-

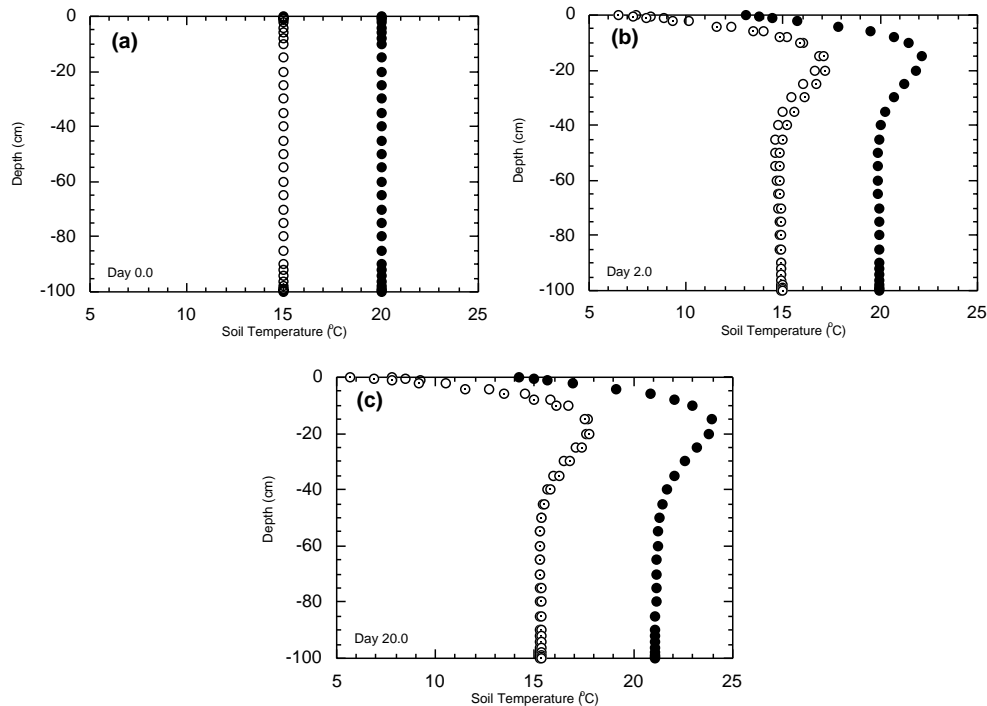


Fig. 4. Comparison of simulated soil temperature profiles using direct insertion for the surface node (open circle) with the true soil temperature profile (solid circle) and the open loop soil temperature profile (open circle with dot) for hourly observations. Soil temperature with depth for times after the beginning of simulation: (a) time zero, (b) 2 days and (c) 20 days.

ever, the depth of update controls the amount of extra mass that is added to the system for redistribution to deeper depths. Thus, it is this limited supply of extra mass which can be added to the system in the direct insertion approach which makes the effect of observation depth so pronounced.

Full retrieval of the soil moisture profile using the direct insertion algorithm is shown in Fig. 3 to take more than 20 days for an observation depth of 1 cm, approximately 12 days for an observation depth of 4 cm and approximately 8 days for an observation depth of 10 cm. These retrieval times are significantly greater than those for the continuous Dirichlet boundary condition (see Table 2), especially for shallower observation depths, indicating that the extra mass being added to the system through the depth of the update is more dominant than the “effective” Dirichlet boundary condition of the update. Fig. 3 also indicates that profile retrieval occurs approximately twice as quickly for observations over 4 cm compared to 1 cm and approximately twice as quick again for observations over 10 cm.

### 5.3.2. Kalman filter

The Kalman filter assimilation scheme performs an instantaneous update of the entire profile every hour, based on the relative magnitudes of the covariances of the observations and the model prediction. Thus, it has the advantage over the direct insertion assimilation

scheme of being able to add or subtract mass from the system from more than just the surface nodes. However, the values assigned to the initial state covariance matrix, observation noise and system noise can have a significant effect on the profile retrieval.

In this study, the initial state covariance matrix was given a value of  $(1000000 \text{ cm}^2, \text{ }^\circ\text{C}^2)$  on the diagonal elements and zero on the off-diagonal elements, representing a large uncertainty in the initial profile values and no correlation between nodes. The observation variances were given a value of 2% of the observed state (matric head or soil temperature) for the diagonal elements and zero for the off-diagonal elements. The system noise was given a value of 5% of the change in system states for that particular timestep on the diagonal elements, rather than 5% of the actual state as indicated by Entekhabi et al. [13], and zero for the off-diagonal elements. The reason for this was that adding 5% of the state to the diagonal element of the system covariance matrix at each timestep, independently of timestep size and time between observations, results in extremely large and unrealistic covariances.

Fig. 5 indicates that profile retrieval proceeds more quickly as the observation depth is increased. However, there is only a small time difference between complete soil moisture profile retrieval for observations at the surface node and an observation depth of 10 cm. The updated moisture profile for the very first update at time

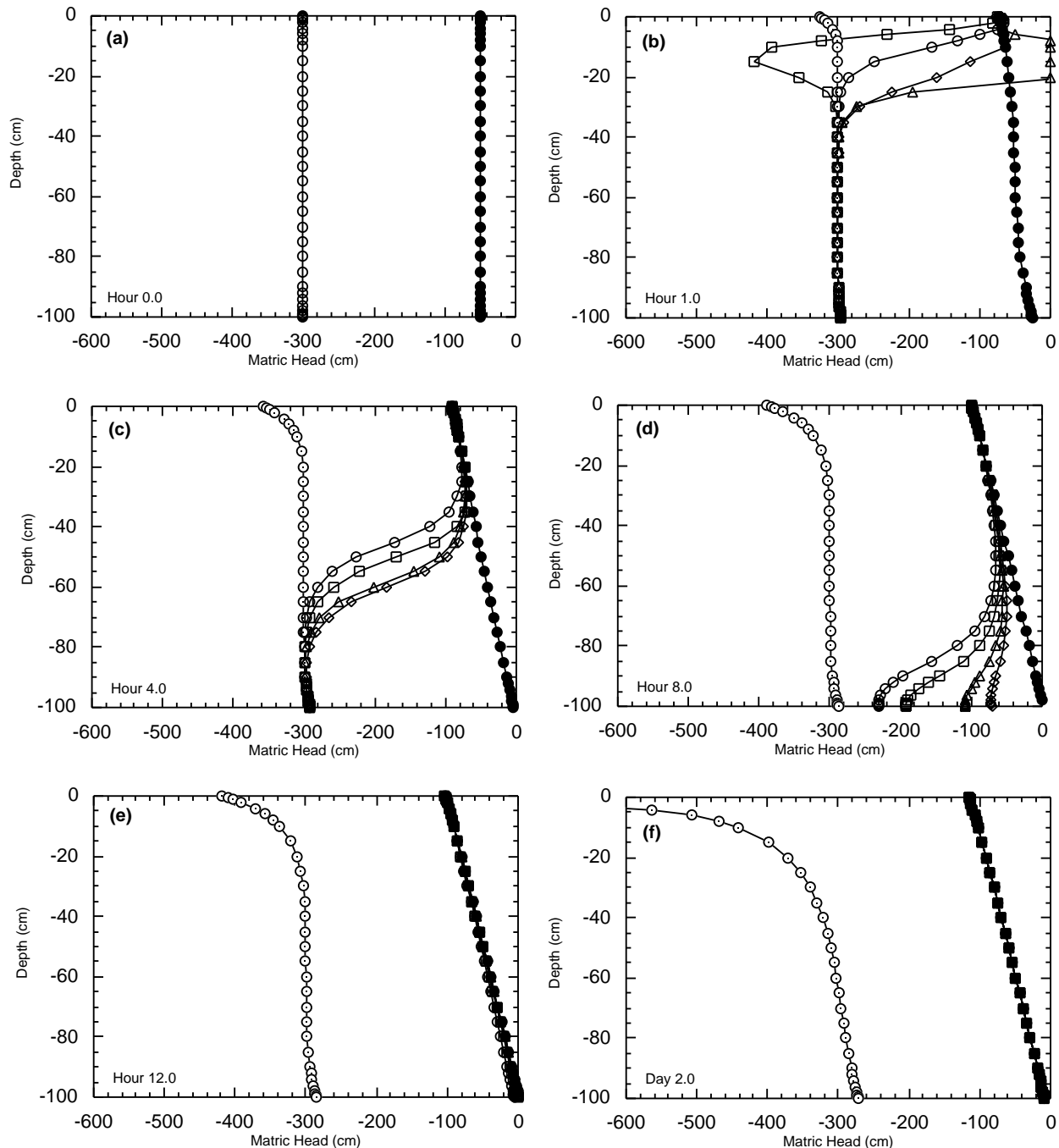


Fig. 5. Comparison of simulated soil moisture profiles using the Kalman filter for observation depths of 0 (open circle), 1 (open square) and 10 cm (open diamond) with the true soil moisture profile (solid circle) and the open loop soil moisture profile (open circle with dot) for hourly observations; initial state variances  $1000000 \text{ cm}^2$ , observation variances 2% of observations and system noise 5% of change in states. Soil moisture with depth for times after the beginning of simulation: (a) time zero, (b) 1 h, (c) 4 h, (d) 8 h, (e) 12 h and (f) 2 days.

1 h contains some artifacts, which are not present in later updates. These artifacts are likely to be a result of the initial state covariances and the poor initial guess. However, as the retrieval algorithm proceeds, the state covariance matrix is “warmed up” and the difference between the forecast surface states and observations becomes less, so that a more uniform and systematic

progression towards the true profile is achieved. As the updating progresses, the Kalman filter continues to make adjustments to the profile at deeper depths until the true profile has been retrieved, at which stage the retrieval algorithm continues to track the true profile.

Full soil moisture profile retrieval using the Kalman filter required approximately 12 h, independent of ob-

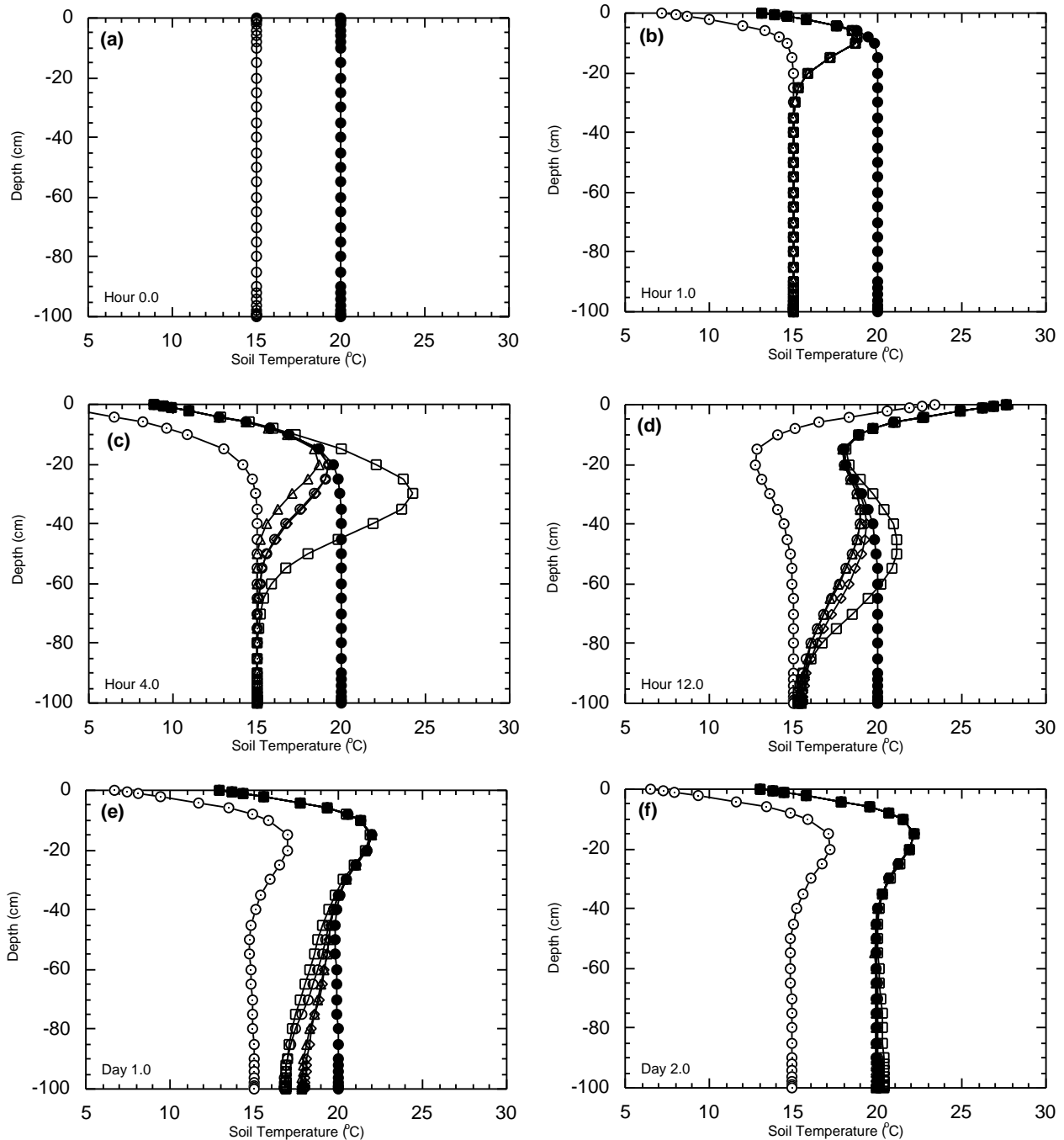


Fig. 6. Comparison of simulated soil temperature profiles using the Kalman filter for observations of the surface node (open symbols) with the true soil temperature profile (solid circle) and the open loop soil temperature profile (open circle with dot) for hourly observations. Retrieved profiles correspond with moisture profile retrieval for observation depths of 0 (open circle), 1 (open square), 4 (open triangle) and 10 cm (open square); initial state variances  $1\,000\,000^{\circ}\text{C}^2$ , observation variances 2% of observations and system noise 5% of change in states. Soil temperature with depth for times after the beginning of simulation: (a) time zero, (b) 1 h, (c) 4 h, (d) 12 h, (e) 1 day and (f) 2 days.

servation depth (including observations at only the surface node). This is compared to 8 days for the direct insertion algorithm with observations over a depth of 10 cm, and no retrieval for observations at the surface node. Full retrieval of the soil temperature profile using the Kalman filter required approximately 2 days com-

pared with no retrieval for the direct insertion. These simulations show that profile retrieval using the Kalman filter is a result of profile updating over depths greater than the observation depth, and is not due to the “effective” Dirichlet boundary condition.

Comparing these results with those of Entekhabi et al. [13], their soil moisture profiles have dried much more quickly than the simulations here, presumably as a result of differences in application of the boundary conditions. In addition, convergence of our retrieved profile towards the true profile progressed from the surface down, rather than from the bottom of the profile up, as seen in Entekhabi et al. [13]. An upward convergence is counter intuitive as the updating is made using observations of the near-surface, meaning that this near-surface information should be passed down the profile. Downward convergence is also seen in the results of Galantowicz et al. [15]. Moreover, Kalman filter retrieval of moisture profiles in this study was achieved more quickly than by Entekhabi et al. [13], approximately 5 days as compared to our 12 h.

As the observations used by Entekhabi et al. [13] for profile retrieval were simulated brightness and thermal infra-red temperatures, and the observations used here were the system states (matric head and soil temperature) for a given observation depth, the observation noise for these two situations are different. In addition, it is unclear how Entekhabi et al. [13] applied their system noise, and what value was assigned to the initial profile variances. These three factors contribute to the differences observed between the results here and of Entekhabi et al. [13].

#### 5.4. Updating once every 5 days

An observation frequency of once every hour is unrealistic for any practical application of profile retrieval from remote sensing observations. At best we may expect a repeat coverage of once every day. However, a repeat coverage of once every 5 days or greater is more probable, at least for the near future. Therefore the direct insertion and Kalman filter assimilation schemes were investigated for their ability to retrieve moisture and temperature profiles with observations once every 5 days.

##### 5.4.1. Direct insertion

It was shown in the previous simulations that a mass/heat balance problem existed with the direct insertion assimilation scheme, particularly for observations at the surface node alone. To alleviate this mass/heat balance problem, a continuous Dirichlet boundary condition was applied for a period of 1 day after the direct insertion update. In applying this boundary condition, the soil moisture observation was held fixed over the 24-h period while the temperature observation was altered for each hour of the 24-h period. The justification for this is that soil moisture does not generally change by more than a few percent during the course of the day, unless it is raining. However, soil surface temperature presents a strong diurnal variation, which needs to be accounted

for. Thus, the assumption made is that the diurnal soil surface temperature variation can be modelled throughout the course of the day, based on the one time-of-day measurement. It was not necessary to be able to model this diurnal variation in such a way for the preliminary investigations given here, as we were primarily interested in testing the idea. Hence, the true surface soil temperature values were used for adjusting the continuous Dirichlet boundary condition each hour.

Simulation results from the direct insertion algorithm are given in Fig. 7 (soil moisture) and Fig. 8 (soil temperature). These results assert the obvious advantage of knowing the true surface soil moisture and temperature values for a greater period of time (compare with Figs. 3 and 4). As indicated previously, the observation depth is not as significant for the direct insertion retrieval algorithm with a continuous Dirichlet boundary condition, due to the mass change being more dependent on the length of time for which the Dirichlet boundary condition is applied than on the depth over which it is applied. Thus, only minimal differences are observed in the retrieved moisture profiles, with full profile retrieval taking approximately 40 days for an observation depth of 10 cm. The soil temperature profile is also fully retrieved after approximately 40 days, with true and retrieved profiles differing by approximately 0.5°C at depth.

As the effectiveness of profile retrieval using the direct insertion retrieval algorithm is determined by the length of time over which a continuous Dirichlet boundary condition is applied after the update, especially as the time between observations is increased, it was felt to be advantageous to identify if there was a simple relationship between update interval and length of time for Dirichlet boundary condition, in order to achieve the same rate of profile retrieval. To investigate this, the Dirichlet boundary condition was applied for a fixed proportion of the update interval. Thus, updates were made every day, 2 and 4 days, with a continuous Dirichlet boundary condition for 1, 2 and 4 h, respectively. The results from these simulations showed conclusively that the relationship between update interval and the proportion of update interval for which a Dirichlet boundary condition must be applied in order to achieve the same profile retrieval rate with the direct insertion retrieval algorithm is not constant. In fact, it was found that as the interval between observations was increased, knowledge of the true surface soil moisture and temperature was required for a greater proportion of the update interval. This highlights the greater importance of more frequent observations, than of the length of time for which knowledge of the true surface states are available.

##### 5.4.2. Kalman filter

Profile retrieval simulations using the Kalman filter retrieval algorithm were initially commenced with the

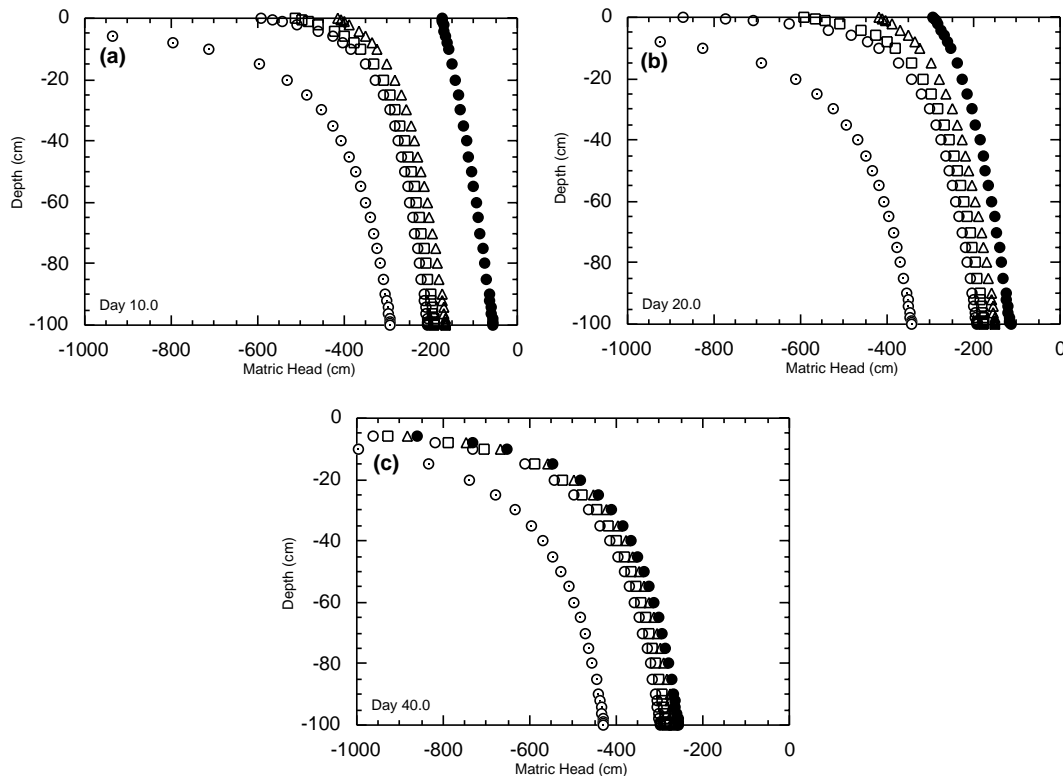


Fig. 7. Comparison of simulated soil moisture profiles using direct insertion with a Dirichlet boundary condition for 1 day over observation depths of 1 (open circle), 4 (open square) and 10 cm (open triangle) with the true soil moisture profile (solid circle) and the open loop soil moisture profile (open circle with dot) for observations each five days. Soil moisture with depth for times after the beginning of simulation: (a) 10 days, (b) 20 days and (c) 40 days.

same initial state variance and noise as used in hourly updating simulations. This however yielded very poor updates of the moisture profile, due to poor forecasting of the model covariance matrix and consequently difficulty updating the states. This was a result of linearisation of an extremely nonlinear model.

In order to achieve a stable update of the moisture profile, it was necessary to reduce the initial state covariance to 10, 5 and 15 cm<sup>2</sup> for observation depths of 1, 4 and 10 cm, respectively. Reduction of the initial state variances to such low values forced the Kalman filter to weight to the model estimate more than the observation. Thus, full retrieval was achieved after approximately 30 days for the 10 cm observation depth, with the retrieval for shallower observation depths proceeding more slowly. Such small values for the initial state variance indicated a unrealistically high confidence in the poor initial estimate. Furthermore, satisfactory profile retrieval was strongly dependent on the initial state variance, with large differences in the soil moisture profile retrieved for slight changes in the initial state variance.

### 5.5. Improved heuristics for the Kalman filter

In view of these stability issues, improvements in the Kalman filter assimilation scheme were explored: (i) use of quasi observations to constrain the update of deeper depths; (ii) log transformation to reduce the difference between the observations and the model forecast; and (iii) volumetric soil moisture transformation to reduce the nonlinearity of the soil moisture profile, particularly near the soil surface, and to reduce the difference between observation and model forecast.

#### 5.5.1. Quasi observations

Near-surface observations of soil moisture are indicative of the soil moisture at depth. Thus, it was proposed to apply the actual observations over the observation depth, and “quasi” observations to the remainder of the moisture profile, as illustrated in Fig. 9. The quasi observations could either be: (i) the observed soil moisture at the observation depth; or (ii) an extrapolation of the soil moisture observation at the observation depth by the steady-state assumption. We chose to apply the steady-state assumption, as this has been shown to be a reasonable approximation under low flux conditions [20]. To account for the greater uncer-

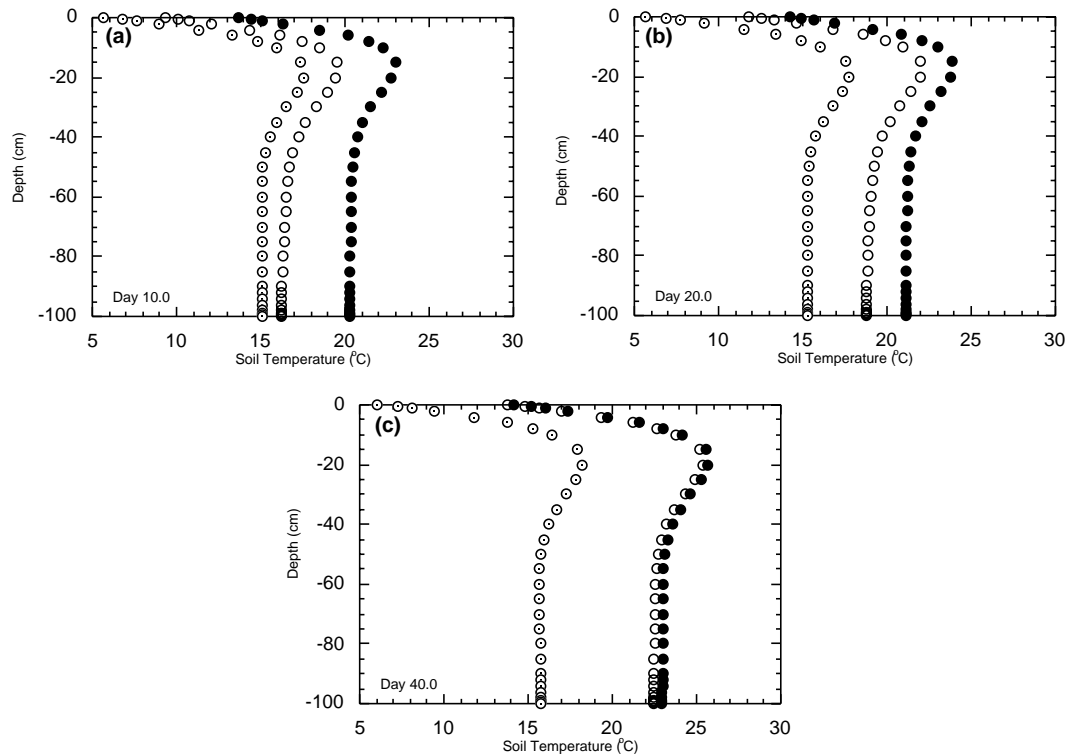


Fig. 8. Comparison of simulated soil temperature profiles using direct insertion with a Dirichlet boundary condition for 1 day at the surface node (open circle) with the true soil temperature profile (solid circle) and the open loop soil temperature profile (open circle with dot) for observations each five days. Soil temperature with depth for times after the beginning of simulation: (a) 10 days, (b) 20 days and (c) 40 days.

tainty associated with the quasi observations, there was a quantile jump applied to the variance of the quasi observation immediately below the observation depth, relative to the variance of the actual observations. An increasing quasi observation variance with depth was then applied (see Fig. 9).

Results using the quasi observations are given in Fig. 10 (soil moisture) and Fig. 11 (soil temperature). These results show that full retrieval of the soil moisture profile is realised after 10 days (two updates) whilst full re-

trieval of the soil temperature profile is realised after 15 days. This is compared with 40 days for soil moisture and temperature retrieval using direct insertion with an observation depth of 10 cm and Dirichlet boundary condition for 1 day. This again shows the advantage of the Kalman filter. However, the quasi observation Kalman filter still has problems. Once full profile retrieval is achieved, the Kalman filter retrieval algorithm continues to track the true profiles until day 30, when the retrieved soil moisture profile drifts from the true profile. This is caused by the departure of the true profile from steady state with largely negative matric heads near the surface. Under field conditions the situation would be unlikely, as evaporation would not occur at a constant rate, so allowing capillary rise during periods of low evaporation. Thus, this departure from the true profile at later updates does not warrant major concern.

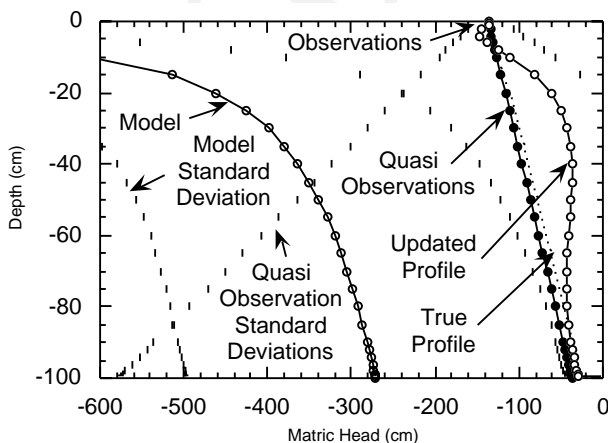


Fig. 9. Illustration of the Kalman filter using quasi observations.

### 5.5.2. Log transformation

Whilst application of quasi observations to the remainder of the un-observed moisture profile was required in order to provide stability to the Kalman filter update for the 5-day observation period, temperature profiles could still be easily retrieved with only the surface observation. It would appear from this, that so long as the observations are not too far from the forecast system states, the Kalman filter could provide a stable

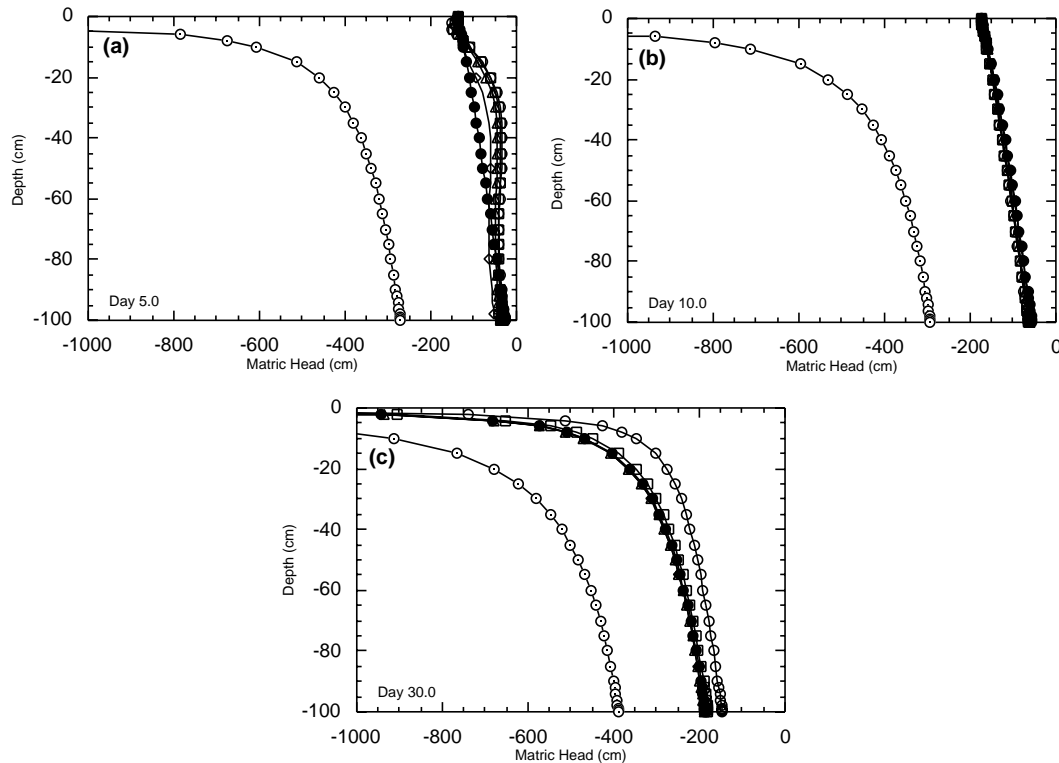


Fig. 10. Comparison of simulated soil moisture profiles using the Kalman filter for observation depths of 0 (open circle), 1 (open square), 4 (open triangle) and 10 cm (open diamond) with the true soil moisture profile (solid circle) and the open loop soil moisture profile (open circle with dot) for observations every 5 days; quasi observations over remainder of profile with variances varying from 20% to 400% of observations. Initial state variances of 1 000 000 cm<sup>2</sup>, observation variances 2% of observations and system noise 5% of states per hour. Soil moisture with depth for times after the beginning of simulation: (a) 5 days, (b) 10 days and (c) 30 days.

update. Thus, if the difference between the observed and forecast moisture values could be reduced, it may be possible to retrieve the moisture profile using only the moisture observations down to the observation depth. One way in which this difference can be achieved is through a log transformation of the matric head (Fig. 12). Both observations and forecast system states and their covariances were transformed into log space. After the update, the updated system states and their covariances were transformed back into the original system [5].

Using the log transformation, it was possible to achieve stable profile retrieval using the 1-cm observation depth without quasi observations, for an initial state variance of 1 000 000 cm<sup>2</sup>, system state noise of 15% of the states per hour, and observation noise of 2% of the observations. Full profile retrieval was achieved after 10 days. However, the first update (day 5) was very sensitive to the initial state variance and the system state noise, with other values providing unstable updates as before.

### 5.5.3. Volumetric moisture transformation

Whilst the log transformation reduced the difference between the observations and model predictions, the transformed profile maintained the large gradient of

matric head with depth near the surface. However, the corresponding volumetric soil moisture profile does not exhibit this same feature, as soil moisture is constrained by the residual soil moisture and porosity. Thus, a soil moisture transformation reduces the difference between observations and model predictions, as well as the nonlinearity of the profile, particularly in the vicinity of the near-surface observations.

The problem associated with transforming matric head into volumetric soil moisture is the assumption of normality. That is, when the soil moisture approaches the residual soil moisture or the porosity, the transformation of the covariances from matric head to volumetric soil moisture [32] predicts that the standard deviation should be small, as volumetric soil moisture cannot be less than the residual soil moisture or greater than the porosity. What is not recognised is that the forecast soil moisture may be much wetter in the dry case or much drier in the wet case. The problem that this creates is that the Kalman filter interprets these small standard deviations as a high degree of certainty in the model prediction and ignores the observation. To overcome this, a limit was placed on the minimum value for  $\partial\theta/\partial\psi$  to ensure that reasonably large standard deviations were maintained for the transformed system

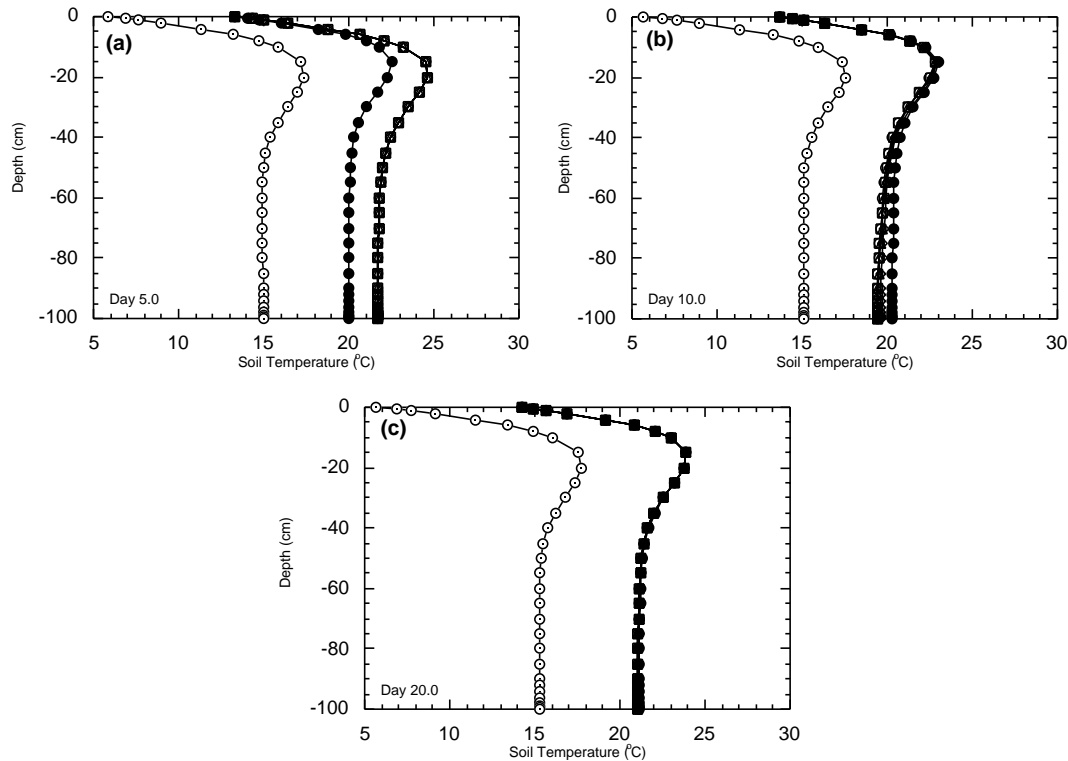


Fig. 11. Comparison of simulated soil temperature profiles using the Kalman filter for observations of the surface node (open symbols) with the true soil temperature profile (solid circle) and the open loop soil temperature profile (open circle with dot) for updates every 5 days. Retrieved profiles correspond with moisture profile retrieval for observations of 0 (open circle), 1 (open square), 4 (open triangle) and 10 cm (open diamond); initial state variances of  $1000000^{\circ}\text{C}^2$ , observation variances 2% of observations and system noise 5% of states per hour. Soil temperature with depth for times after the beginning of simulation: (a) 5 days, (b) 10 days and (c) 20 days.

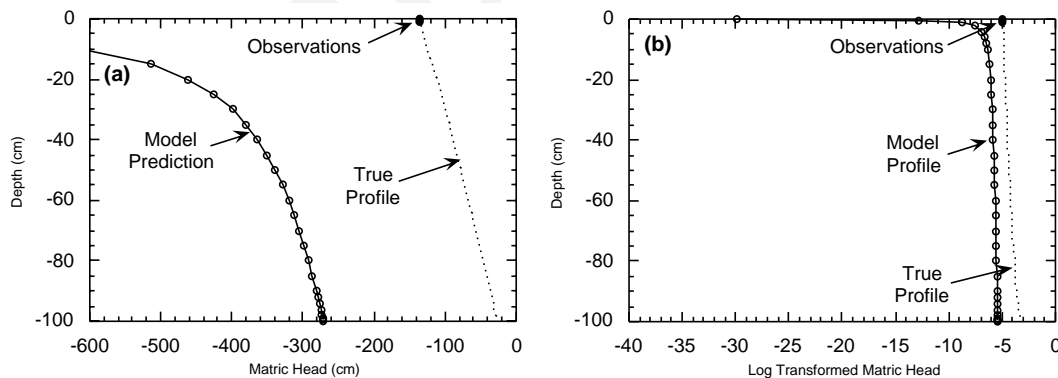


Fig. 12. Illustration of log normal transformation of the matric head: (a) pre-transformation and (b) post-transformation.

states near the soil surface, while ensuring that the standard deviation was not greater than the porosity.

Using this moisture transformation, stable profile retrieval was obtained for all observation depths apart from the case of the surface node alone. The reason for not being able to obtain retrieval for surface node observations was that the transformation process resulted in a low correlation with forecast soil moisture at deeper depths. The results from these simulations (Fig. 13)

show that full retrieval of the soil moisture profile was realised after 10 days for the 10-cm observation depth and 15 days for 1 and 4 cm observation depths. A larger initial state variance was used for the 1-cm observation depth ( $1000000 \text{ cm}^2$ ) than for the 4 and 10 cm observation depths ( $10000 \text{ cm}^2$ ) to ensure comparable standard deviations were obtained for surface nodes after the transformation. Retrieval rates were slightly slower than the quasi observation retrieval, which required 10

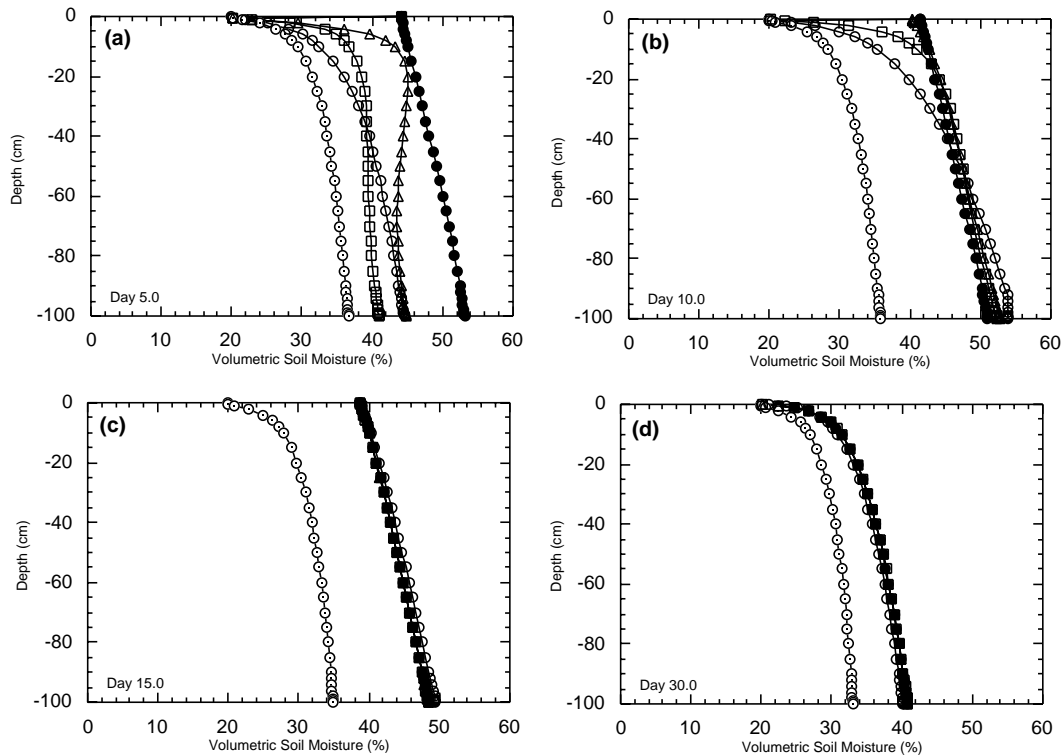


Fig. 13. Comparison of simulated soil moisture profiles using the Kalman filter for observation depths of 1 (open circle), 4 (open square), and 10 cm (open triangle) with the true soil moisture profile (solid circle) and the open loop soil moisture profile (open circle with dot) for updates every 5 days; moisture transformation of states and state covariances. Initial state variances of 1000000, 10000 and 10000 cm<sup>2</sup>, observation variances 2% of observations and system noise 5% of states per hour. Soil moisture with depth for times after the beginning of simulation: (a) 5 days, (b) 10 days, (c) 15 days and (d) 30 days.

days. Hence, only one extra update was required using the moisture transformation. Furthermore, had soil moisture been the dependent state in the model, profile retrieval may have been achieved more rapidly, as the transformation of covariances and its associated problems and assumptions would be eliminated. Thus, while the  $\psi$ -based form of the moisture equation is a better representation of the soil moisture profile and its dynamics, the  $\theta$ -based form is required for stable updating with the Kalman filter when the soil becomes dry or observations and model predictions are very different. Finally, the retrieved profile converged towards the true profile at depth rather than at the surface. This was a result of the covariance transformation.

## 6. Conclusions

It has been shown that the Kalman filter assimilation scheme is superior to the direct insertion assimilation scheme. Profile retrieval was unsuccessful for direct insertion using the surface node alone, with observations over some non-zero depth being required. The superiority of the Kalman filter lies in its ability to adjust the entire profile, whilst direct insertion can only directly

alter the profile within the observation depth. However, the Kalman filter can only do this if there is a high correlation between the soil moisture of adjacent depths. Thus, the unsaturated soil moisture model used for this purpose must be a function of the soil moisture of adjacent nodes, so that correlations between adjacent layers will be evolved by the covariance forecasting equation.

Being unable to directly alter more than the observed soil moisture values means that mass/heat imbalance cannot be readily corrected by direct insertion, as the mass/heat added during an instantaneous direct insertion update is restricted by the depth of the observation. Thus, an increased observation depth is an advantage for the direct insertion assimilation scheme. As the observations become less frequent, the direct insertion retrieval algorithm requires a continuous Dirichlet boundary condition, which must be applied for an increasingly longer proportion of the update interval. Again, this results from the mass/heat balance. This would indicate that more frequent observations are more useful for profile retrieval than knowledge of the surface observations for a greater period of time. The mass added during a continuous Dirichlet boundary condition is constrained by the physical rate at which

moisture can be transferred through the profile, and the length of time for which the continuous Dirichlet boundary condition is maintained. Thus, the observation depth has a reduced influence on the retrieval time when the Dirichlet boundary condition is applied.

It has been shown that observation depth does not have a significant effect on the profile retrieval time for the Kalman filter assimilation scheme. This is because the Kalman filter is able to modify the soil moisture below the observation depth due to the correlation between soil moisture states at depth. However, it has been observed that unrealistic updating of the profile can occur when observations become less frequent, the observed and modelled profiles are far apart, there is a large uncertainty in the modelled profiles, and the model state profile is extremely nonlinear in the vicinity of the observation. This again highlights the importance of frequent observations, and suggests that for the Kalman filter assimilation scheme, repeat coverage frequency is more important than observation depth. It has also been shown that the Kalman filter retrieval algorithm is less susceptible to unstable updates if volumetric soil moisture is modelled as the dependent state.

This desktop study has shown that surface soil moisture data is useful for correcting errors in simulated soil moisture profiles as a result of poor initialisation. Moreover, future studies should concentrate their efforts on the use of statistical assimilation schemes such as the Kalman filter, which have the ability to make corrections to the unobserved portion of the soil profile directly. However, the soil moisture model used for application of the Kalman filter should be as linear a representation of the soil physical processes as possible, such as the  $\theta$ -based Richards' equation. Having shown the usefulness of assimilating surface soil moisture, the advantages of the Kalman filter over direct insertion and the potential problems that may be encountered with the Kalman filter, this study has paved the way for a field application of the Kalman filter assimilation scheme, which will be discussed in a forthcoming paper.

### Acknowledgements

This work has been funded in part by an Australian Postgraduate Award scholarship and in part by the Hunter Water Corporation.

### References

- [1] Axelsson SRJ, Klemedtsson L, Robertson K, Rosswall T. Remote sensing techniques for monitoring soil moisture and denitrification activity of arable land. In: Proceedings of the International Symposium on Remote Sensing. Bangkok, Thailand; 1990. p. 465–77.
- [2] Bear S. Hydraulics of ground water. New York: McGraw-Hill; 1979. p. 569.
- [3] Beecham R. Patterns of spatial and temporal variability of factors affecting nutrient export from Chaffey dam catchment. In: Binning P, Bridgman H, Williams B, editors. MODSIM '95 International Congress in Modelling and Simulation. Newcastle; 1995; p. 183–87.
- [4] Beven KJ, Fisher J. Chapter 1: Remote sensing and scaling in hydrology. In: Stewart JB, Engman ET, Feddes RA, Kerr Y, editors. Scaling up in hydrology using remote sensing. New York: Wiley; 1996. p. 1–18.
- [5] Bras RL, Rodriguez-Iturbe I. Random functions and hydrology. Reading, MA: Addison-Wesley; 1985. p. 559.
- [6] Cary JW, Taylor SA. Chapter 13: The dynamics of soil water, Part II – Temperature and solute effects. In: Hagan RM, Haise HR, Edminster TW, editors. Irrigation of agricultural lands. Madison, USA: American Society of Agronomy; 1967. p. 245–53.
- [7] de Vries DA. Simultaneous transfer of heat and moisture in porous media. *Trans Am Geophys Union* 1958;39(5):909–16.
- [8] de Vries DA. Chapter 7: Thermal properties of soils. In: van Wijk WR, editor. Physics of plant environment. New York: Wiley; 1963. p. 210–35.
- [9] D'Urso G, Giacomelli A, Mancini M, Troch PA. The SESAR '93 experience on soil dielectric behaviour from ERS-1 satellite. In: DeTroch FP, Su Z, Troch PA, editors. First workshop on data collection and data analysis issues for spatial and temporal soil moisture mapping from ERS-1 and JERS-1 SAR data and macroscale hydrologic modelling (EV5V-CT94-0446). Institute for Agricultural hydraulics, University of Naples, Italy; 1994. p. 1–13.
- [10] Engman ET. Progress in microwave remote sensing of soil moisture. *Can J Remote Sensing* 1990;16(3):6–14.
- [11] Engman ET, Chauhan N. Status of microwave soil moisture measurements with remote sensing. *Remote Sensing Environ* 1995;51(1):189–98.
- [12] Entekhabi D, Nakamura H, Njoku EG. Retrieval of soil moisture profile by combined remote sensing and modeling. In: Choudhury BJ, Kerr YH, Njoku EG, Pampaloni P, editors. ESA/NASA International Workshop on Passive Microwave Remote Sensing Research Related to Land Atmosphere Interactions. France: St. Lary; 1993. p. 485–98.
- [13] Entekhabi D, Nakamura H, Njoku EG. Solving the inverse problem for soil moisture and temperature profiles by sequential assimilation of multifrequency remotely sensed observations. *IEEE Trans Geosci Remote Sensing* 1994;32(2):438–48.
- [14] Feddes RA, Menenti M, Kabat P, Bastiaanssen WGM. Is large-scale inverse modelling of unsaturated flow with areal average evaporation and surface soil moisture as estimated from remote sensing feasible?. *J Hydrol* 1993;143:125–52.
- [15] Galantowicz J, Entekhabi D, Njoku E. Tests of sequential data assimilation for retrieving profile soil moisture and temperature from observed L-band radiobrightness. *IEEE Trans Geosci Remote Sensing* 1999;37(4):1860–70.
- [16] Georgakakos KP, Baumer OW. Measurement and utilization of on-site soil moisture data. *J Hydrol* 1996;184:131–52.
- [17] Georgakakos KP, Smith GF. On improved hydrologic forecasting – Results from a WMO real-time forecasting experiment. *J Hydrol* 1990;114:17–45.
- [18] Giacomelli A, Bacchiega U, Troch PA, Mancini M. Evaluation of surface soil moisture distribution by means of SAR remote sensing techniques and conceptual hydrological modelling. *J Hydrol* 1995;166:445–59.
- [19] Houser PR, et al. Integration of soil moisture remote sensing and hydrologic modeling using data assimilation. *Water Resour Res* 1998;34(12):3405–20.
- [20] Jackson TJ. Profile soil moisture from surface measurements. *J Irrigation Drainage Div, Proc ASCE* 1980;106 (IR2):81–92.

- [21] Jackson TJ. Survey of applications of passive microwave remote sensing for soil moisture in the USSR. *EOS Trans Am Geophys Union* 1982;63(19):497–9.
- [22] Jackson TJ. III. Measuring surface soil moisture using passive microwave remote sensing. *Hydrol Process* 1993;7:139–52.
- [23] Jackson TJ, Hawley ME, O'Neill PE. Preplanting soil moisture using passive microwave sensors. *Water Resour Bull* 1987;23(1):11–9.
- [24] Jackson TJ, Schmugge TJ, Engman ET. Remote sensing applications to hydrology: soil moisture. *J Hydrol Sci* 1996;41(4):517–30.
- [25] Jackson TJ, Schmugge TJ, Nicks AD, Coleman GA, Engman ET. Soil moisture updating and microwave remote sensing for hydrological simulation. *Hydrol Sci Bull* 1981;26(3):305–19.
- [26] Kimball BA, Jackson RD, Reginato RJ, Nakayama FS, Idso SB. Comparison of field-measured and calculated soil heat fluxes. *Soil Sci Soc Am J* 1976;40(1):18–25.
- [27] Klute A. Chapter 2: soil water flow theory and its application in field situations. In: Bruce RR, et al., editors. *Field soil water regime*, SSSA Special Publication No. 5. Madison, USA: Soil Science Society of America; 1973. p. 9–35.
- [28] Lakshmi V, Susskind J. Land surface hydrological processes using satellite data. In: Stein TI, editor. *International Geoscience and Remote Sensing Symposium*, Singapore; 1997. p. 1102–04.
- [29] Lin DS, Wood EF, Troch PA, Mancini M, Jackson TJ. Comparisons of remotely sensed and model-simulated soil moisture over a heterogeneous watershed. *Remote Sensing Environ* 1994;48:159–71.
- [30] Mancini M, Troch P. Experimental set-up for soil moisture profile determination using multi-frequencies back-scattering data. *EMSL Newsletter*; 1995.
- [31] Mancini, et al., M. Experimental setup at the EMSL for retrieval of soil moisture profiles using multifrequency polarimetric data. *International Geoscience and Remote Sensing Symposium*, Firenze, Italy, 1995; p. 2023–25.
- [32] Mikhail EM, Ackerman F. *Observations and least squares*. New York: IEP; 1976; p. 497.
- [33] Milly PCD. A mass-conservative procedure for time-stepping in models of unsaturated flow. *Adv Water Resour* 1985;8:32–6.
- [34] Newton RW, Heilman JL, van Bavel CHM. Integrating passive microwave measurements with a soil moisture/heat flow model. *Agri Water Management* 1983;7:379–89.
- [35] Peplinski NR, Ulaby FT, Dobson MC. Dielectric properties of soils in the 0.3–1.3 GHz range. *IEEE Trans Geosci Remote Sensing* 1995;33(3):803–7.
- [36] Philip JR. The theory of infiltration: 1. The infiltration equation and its solution. *Soil Sci* 1957;83:345–57.
- [37] Philip JR, de Vries DA. Moisture movement in porous materials under temperature gradients. *Trans Am Geophys Union* 1957;38(2):222–32.
- [38] Saha SK. Assessment of regional soil moisture conditions by coupling satellite sensor data with a soil-plant system heat and moisture balance model. *Int J Remote Sensing* 1995;16(5):973–80.
- [39] Schmugge T. Chapter 5: remote sensing of soil moisture. In: Anderson MG, Burt TP, editors. *Hydrological forecasting*. New York: Wiley; 1985. p. 101–24.
- [40] Su Z, Troch PA, de Troch FP, Nochttergale L, Cosyn B. Preliminary results of soil moisture retrieval from ESAR (EMAC 94) and ERS-1/SAR, Part II: Soil moisture retrieval. In: De Troch, FP, Troch PA, Su Z, Cosyn B, editors. *Second workshop on hydrological and microwave scattering modelling for spatial and temporal soil moisture mapping from ERS-1 and JERS-1 SAR data and macroscale hydrologic modelling (EV5V-CT94-0446)*, Institute National de la Recherche Agronomique, Unité de Science du Sol et de Bioclimatologie, France; 1995. p. 7–19.
- [41] Topp GC, Davis JL, Annan AP. Electromagnetic determination of soil water content: measurement in coaxial transmission lines. *Water Resour Res* 1980;16(3):574–82.
- [42] van Genuchten MT. A closed-form equation for predicting the hydraulic conductivity of unsaturated soils. *Soil Sci Soc Am J* 1980;44:892–8.
- [43] Walker JP, Troch PA, Mancini M, Willgoose GR, Kalma JD. Profile soil moisture estimation using the modified IEM. In: Stein TI, editor. *International Geoscience and Remote Sensing Symposium*. Singapore; 1997. p. 1263–65.